Master Program in Environmental Engineering
Department of Civil Engineering and Geosciences
Delft University of Technology
The Netherlands

Additional Thesis

Towards OMPs Removal: Application of Visible Light Driven Heterojunction Based $BiVO_4$/BiOI Photoanode for the Degradation of Paracetamol Demineralized Water

By
Yiqian Wu
5217806

Supervisor: **Henri Spanjers**
Jan Peter van der Hoek
Agha Zeeshan Ali

July 6 2022

Abstract

Currently, organic micropollutants (OMPs) are continuously and uncontrollably released into the water environment worldwide, as the reason for their special properties, OMPs removal has been a global challenge. This study focus on the acetaminophen degradation by photo-electrolysis (PEC) activities, which is one of the promising advanced oxidation processes (AOP) technolo-gies. First, we report the fabrication methods of the $BiVO_4$/BiOI heterojunction on FTO glass, then characterised the prepared photoanodes with XPS, XRD, SEM, EDS, UV-vis and IPCE. The results demonstrated the $BiVO_4$/BiOI p-n heterojunction had been successfully electrodeposited on the FTO glass. Further, the LSV and EIS analysis in this study showed the $BiVO_4$/BiOI photoanode had less photocurrent density than $BiVO_4$ when carried out in the solution of acetaminophen. Even if the heterojunction did not improve the photocurrent, it significantly enhance the acetaminophen removal efficiency in the PEC degradation process. $BiVO_4$/BiOI photoanode achieved 99% degradation efficiency in 3 hours and obtained $0.019\,min^{-1}$ of the reaction rate constant. Overall, these results indicate that $BiVO_4$/BiOI heterojunction has a great application potential for the degradation of OMPs in the wastewater treatment plants secondary effluent.

Key Words: Organic Micro-pollutants, Photo-eletrocatalysis, Electrodeposition, p-n Heterojunction.

Nomenclature

$OMPs$	Organic Micro-Pollutants
$WWTPs$	Wastewater Treatment Plants
AOP	Advanced Oxidation Process
PEC	Photo-electrocatalyst
PC	Photocatalyst
$k_{\cdot OH}$	Rate constant of each OMPs during the reaction with $\cdot OH$
FTO	Fluorine-doped tin oxide
h^+	Hole
e^-	Electron
SEM	Scanning Electron Microscopy
EDS	Energy-dispersive X-ray Spectrometer
XRD	X-ray Diffraction
XRF	X-ray Fluorescence
XPS	X-ray Photoelectron spectroscopy
$IPCE$	Incident Photo-to-electron Conversion Efficiency
LSV	Linear Sweep Voltammentry
EIS	Electrochemical Impedance Spectroscopy
R_{ct}	Charge-transfer Resistance

Contents

List of Figures

Chapter 1

Introduction

1.1 Organic Micro-pollutants in WWTPs Effluent

In recent years, there has been a worldwide concern in the assessment of clean drinking water. Nevertheless, extensive research has shown that organic micro-pollutants (OMPs) are continuous and uncontrolled released into water, sediment and soil systems[2]. Also, it can be bioaccumulated in plants and other organisms (human or animal) [3]. This fact attracts an increasing concern because of its potential great hazard to both the environment and to human health [4] even at trace level concentrations (ppb). The existing body of research on the source of OMPs suggests that wastewater treatment plants (WWTPs) effluents are the main reason compared to irrigation and runoff in agriculture activities [3]. The WWTPs effluent is the effluent from the secondary clarifiers. As the results of OMPs' special properties, such as low concentration, non-biodegradable and a wide variety, conventional WWTPs can hardly remove them through the activated sludge process [5].

1.2 PEC Technology

Recent evidence suggests that photo electrocatalytic (PEC) technology is a good approach for removing OMPs in WWTPS effluents using semiconducting materials as photoanodes as one of the most promising advanced oxidation processes (AOP) technologies [6]. It is now well established from a variety of studies, that PEC can generate hydroxyl radicals ($\cdot$ OH) in both solar and electric energy. Hydroxyl radicals as a strong oxidant can oxidize OMPs highly and

non-selectively and are capable of mineralizing OMPs [1]. Equations 1.1-1.3 and Figure 1.1 show the mechanism of how PEC activity generates hydroxyl radicals when it happens on a photoanode.

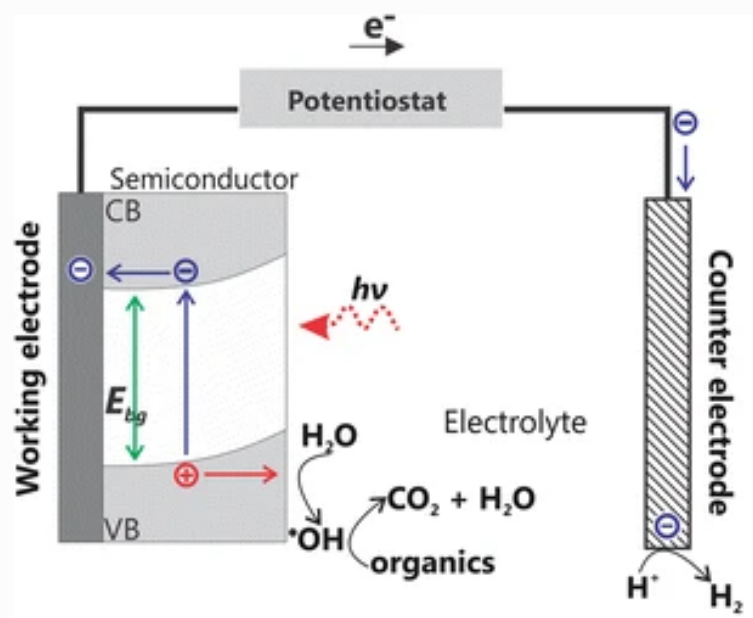

Figure 1.1: PEC activity mechanism and main reactions [1].

$$Absorption\ of\ light : SC + h\nu(> E_g) = e^- + h^+ \tag{1.1}$$

$$\cdot OH\ production : H_2O + h^+ = H^+ + \cdot OH \tag{1.2}$$

$$OMPs\ degradation : OMPs + x \cdot OH = aCO_2 + bH_2O + cNO_3^- + dSO_4^{2-} + eCl^- \tag{1.3}$$

In additional, the applied bias potential helps in driving away photogenerated electrons from the anode surface thereby prolonging the lifetime of photogenerated holes [7]. Therefore, PEC always has higher OMPs removal efficiency than photo-catalysis (PC).

1.3 Photoanode Materials and Fabrication

Studies of Bismuth vanadate ($BiVO_4$) show the importance of its great potential for application in PEC treatment. Previous research has established that $BiVO_4$ is a non-toxic and cheap n-type semiconductor (an impurity mixed semiconductor material used in electronics, the impure atoms give free electrons to the semiconductor) with notable photostability [8]. Generally, $BiVO_4$ has

multiple crystal structures, the most remarkable one is the monoclinic structure, which has a narrow 2.4 eV energy bandgap and a relatively higher OMPs degradation efficiency [9].

Unfortunately, the application of $BiVO_4$ is hampered by the relatively rapid recombination of photoexcited electron-hole pairs and poor charge carrier transport. In order to enhance the PEC activities when using $BiVO_4$, the formation of heterojunction has recently been examined to be one of the outstanding techniques by investigators. Especially, the formation of heterojunction between n-type and p-type semiconductors can highly increase the lifespan of the charge carries by improving the efficiency of both light-harvesting and photogenerated electron-hole pairs separation [10].

Therefore, several attempts have been made to bismuth oxyiodide (BiOI), a p-type bismuth-based semiconductor, which has a small band gap of 1.8 eV [11]. BiOI also has a good prospect for visible light applications, but the high combination rate of its photogenerated electron-hole pairs is a huge problem. It is now well established from a variety of studies, that the p-n $BiOI/BiVO_4$ heterojunction can highly increase the PEC activity. However, up to now, far too little attention has been paid to the application of the p-n $BiOI/BiVO_4$ heterojunction in the PEC degradation when treating a large volume of low concentration OMPs solution.

As for the methods of $BiVO_4$ film fabrication, previous research comparing hydrothermal synthesis, electrodeposition, chemical vapour deposition and metal-organic decomposition has found that a proper fabrication method can lead to a better PEC activity as its better morphology, crystal structure and phase formation [12]. In this study, electrodeposition is chosen as the method of $BiVO_4$ film fabrication, because of its simple operation and stable product quality.

Chapter 2

Methods

2.1 Fabrication of $BiVO_4$ Photoanode

A number of techniques have been developed to obtain the $BiVO_4$ film, herein, we applied the electrodeposition method as it is recently popular and reliable. To prepare the solution for electrodeposition, firstly, we add 0.04 M Bismuth Nitrate Pentahydrate ($Bi(NO_3)_3 \cdot 5H_2O$) to the 0.4 M Potassium Iodide (KI) solution which pH should be adjusted to 1.5-1.6 in advance. Next, mix it with 20 mL of Ethanol (100 %) containing 0.23 M p-benzoquinone under sonicating for 15 min.

To electrodeposited the BiOI film on the FTO glass (40 mm $\times$ 40 mm x 2.2 mm, the surface resistivity of $\sim$ 7 Ω /sq), we applied cathodic bias at -0.2 V to FTO glass under the solution prepared before for 120 s, 300 s, 420 s, 600 s and 900 s respectively. In the electrodeposition process, the FTO glass, Ag/AgCl (3.0 M KCl) electrode and platinum wire were performed as the working electrode, reference electrode and counter electrode correspondingly. Figure 2.1 shows the connection of electrodeposition process.

After rinsing the prepared BiOI electrode several times by deionized water and drying it in the fume hood, a 0.15 - 0.2 mL of Dimethyl Sulfoxide (DMSO) solution containing 0.2 M Vanadyl-Acetylacetonate was dropped onto the electrode surface. Then, the electrode was placed in the furnace at 450 °C for 2 h (ramping rate at 2 °C/min). At last, take it out of the furnance til it totally cooling down to the room temperature, remove the excess V_2O_5 by soaking the electrodes in 1.0 M NaOH solution for 15 min with gentle stirring. Gently washed the prepared $BiVO_4$ film

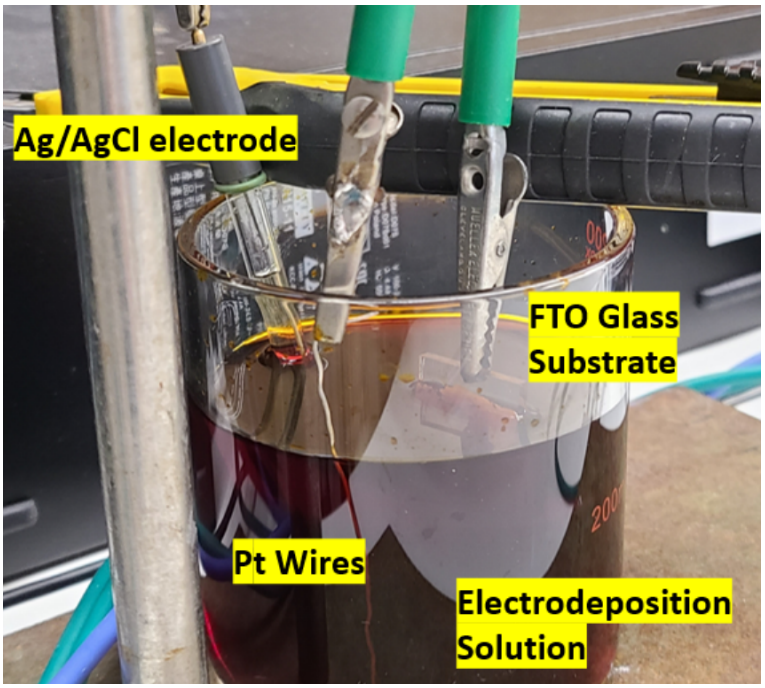

Figure 2.1: The connection of three-electrodes configuration during electrodeposition.

with deionized water several times and dried it in the fume hood.

2.2 Fabrication of $BiVO_4$/BiOI Photoanode

To add an extra BiOI film on the existing $BiVO_4$ film, we still used the electrodeposition method. First of all, choose the best performance electrode which has the highest OMPs removal rate. Then, applied -0.2 v cathodic bias to the prepared $BiVO_4$/FTO in the electrodeposition solution mentioned in Section 2.1 for the same amount of time as the best electrode. As the control group, only BiOI film with the same electrodeposition time should be deposited on the bare FTO glass. Gently washed the prepared $BiVO_4$/BiOI/FTO and BiOI/FTO with deionized water several times and dried it in the fume hood.

2.3 Photoelectrochemical Degradation Experiment

All the electoral data were recorded on an Autolab PGSTAT128N machine with three-electrodes configuration. The prepared photoanode, Ag/AgCl (3.0 M KCl) electrode and carbon electrode were performed as working electrode, reference electrode and counter electrode correspondingly. For the light source, a solar simulator SUNTEST XXL+ with 3 air cooled 1700 W Xenon lamps

(60 W/m^2) has been used in this experiment. As shown in Figure 2.2, the light comes from directly above that the photoanode under the front illumination.

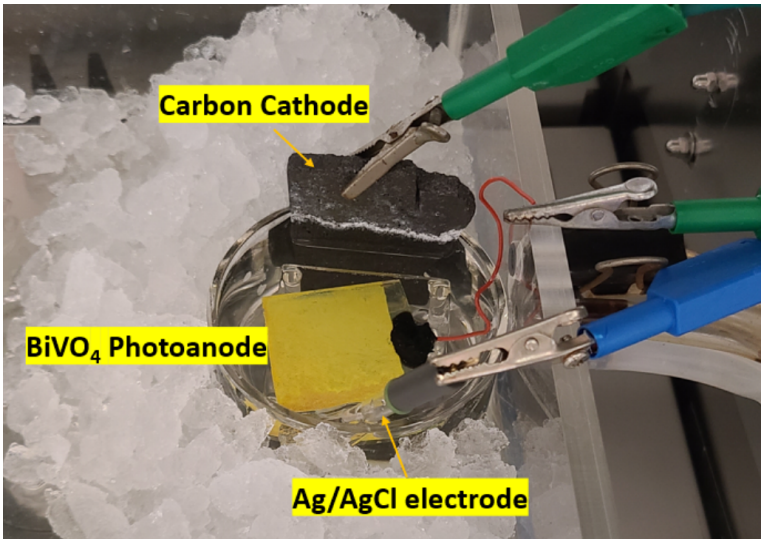

Figure 2.2: The three-electrodes configuration. The bright yellow $BiVO_4$ photoanode under the front illumination. The ice around the reactor aims to minimize the evaporation of solution.

For the photoelectrochemical degradation experiment, the PEC cell contained 167 mL 0.1 M Na_2SO_4 and 40 μg/L acetaminophen solution with a magnetic stirring bar kept mixing under the photoanode during the whole process. Every batch runs for 6 h, with samples taken at hourly intervals by pipette. We place ice surrounding the cell aims to minimize the evaporation of the solution. The acetaminophen concentration was measured by ultra-high performance liquid chromatography-triple quadrupole mass spectrometry (UHPLC-MS/MS) (Waters Acquity UPLC with Quattro micro API Tandem Quadrupole System). As the control groups, BiOI and $BiVO_4$ electrodes have been tested separately in the same environment.

2.4 Characterisation Measurements of Prepared Photoanode

To gain further insight into the characterisation of photoanode, several technologies are applied to analyze. For the morphology of photoanode surface nanostructure, scanning electron microscopy (SEM) (FEI, Quanta F650) coupled with an energy-dispersive X-ray spectrometer (EDS) was followed on FEI Model Quanta 650 Field Emission Scanning Electron Microscope, and the Inca 250 SSD XMax20 detector. The degree of crystallinity and purity of the photoanodes were determined with the X-ray diffraction (XRD) using Cu Kα radiation within a range of 2 θ = 10

^{o} - 130 ^{o}, a step size of 0.040 ^{o} 2 θ, and counting time per step 2 seconds and X-ray fluorescence (XRF) (Panalytical Axios Max WD-XRF spectrometer, SuperQ5.0i/Omnian software).

The optical properties of the prepared photoanodes were studied using UV-vis (The LAMBDA 1050+ UV/Vis/NIR spectrophotometer, UV Winlab software) and incident photon-to-electron conversion efficiency (IPCE), the radiation wavelength range went from 280 nm to 700 nm.

For the electro-analysis, photocurrent, linear sweep voltammetry (LSV) (potential from -0.2 V_{REF} to 1.5 V_{REF}, 0.1 V/s scan rate) and electrochemical impedance spectroscopy (EIS) (applied frequency from 10000 Hz to 0.01 Hz, plots were obtained under both dark and solar condition) were used in a 0.1 Na_2SO_4 and 40 μg/L acetaminophen solution at room temperature.

Chapter 3

Results and Discussions

3.1 Electrodeposition Pre-experiment

Before the formal experiments, the electrodeposition pre-experiments were tested aimed to confirm which electrodeposition conditions can provide the best photoanode. The results obtained from the degradation of acetaminophen are shown in Fig 3.1. Significantly, -0.2 V and 5 min is the best electrodeposition condition compared to -0.2 V 2 min, 7 min, 10 min and 15 min. Besides, when applying longer time than 5 min in the electrodeposition process, the $BiVO_4$ layer became thick and fragile, which might cause it to break into pieces by stirring. Therefore, the only -0.2 V 5 min condition was applied in the following formal experiments.

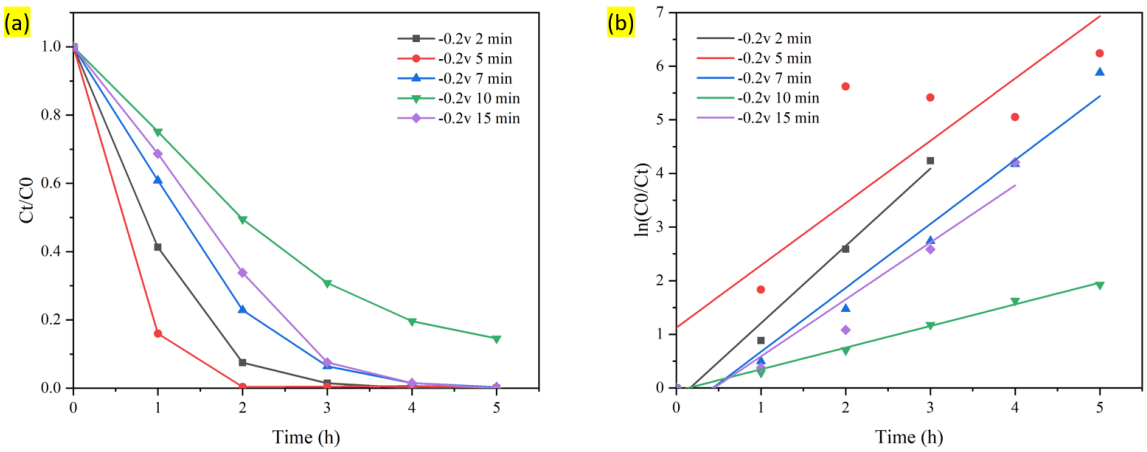

Figure 3.1: (a) Normalized Acetaminophen concentration decay versus time plots, (b) Kinetics plots for degradation of -0.2v 2 min, 5min, 7 min, 10 min and 15 min ED conditions.

3.2 Structual and Morphology characterization of Photoanodes

On a macro level, the colour of the photoanodes is presented in Fig 3.2. The BioI electrode is dark orange, the BiVO4 electrode is bright yellow and the colour of $BiVO_4$/BiOI is combined two of them and shows light orange.

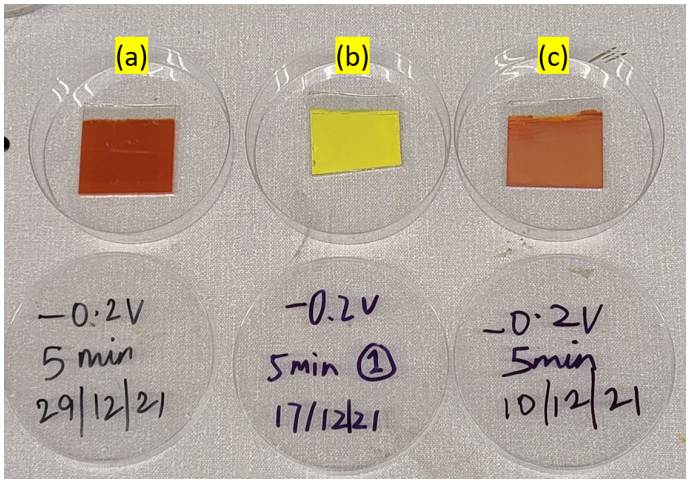

Figure 3.2: Photographs of the photoanodes: (a) BiOI, (b) $BiVO_4$, (c) $BiVO_4$/BiOI.

3.2.1 XPS analysis

The results of the XPS analysis are shown in Fig 3.3, the C 1s peak (binding energy = 284.6 eV) from the adventitious hydrocarbons was used for calibration to determine Bi, V, I, and O. Fig 3.3(a) demonstrated the XPS survey spectra of BiOI, BiVO4, and $BiVO_4$/BiOI, which indicated that BiOI layer was successfully electrodeposited on $BiVO_4$ layer, because only Bi, V, I and O coexisted in $BiVO_4$/BiOI, especially no peaks representing for other elements. Fig 3.3b-e provided the high resolution spectra of Bi 4f, V 2p, I 3d and O 1s which give mere explicit information of chemical state. As can be seen from 3.3(b), the peaks of 163.52 eV and 158.26 eV can be attributed to Bi $4f_{5/2}$ and Bi $4f_{7/2}$, therefore, Bi^{3+} exsited in the photoanodes [13]. The peaks of 520.4 eV and 516.01 eV are presented in Fig 3.3(c), which belonged to V $2P_{2/1}$ and V $2P_{3/2}$ [14]. Also, The peaks of 629.50 eV and 618.16 eV are presented in Fig 3.3(d), which belonged to I $3d_{3/2}$ and I $3d_{5/2}$ [14]. Fig 3.3(e) presented the O 1s peaks from the $BiVO_4$/BiOI photoanode, the peak of 530.22 eV was attributed to Bi-O bonds in BiOI, further, the other peak of 529.08 eV was ascribed to V-O bonds in BiOI [13].

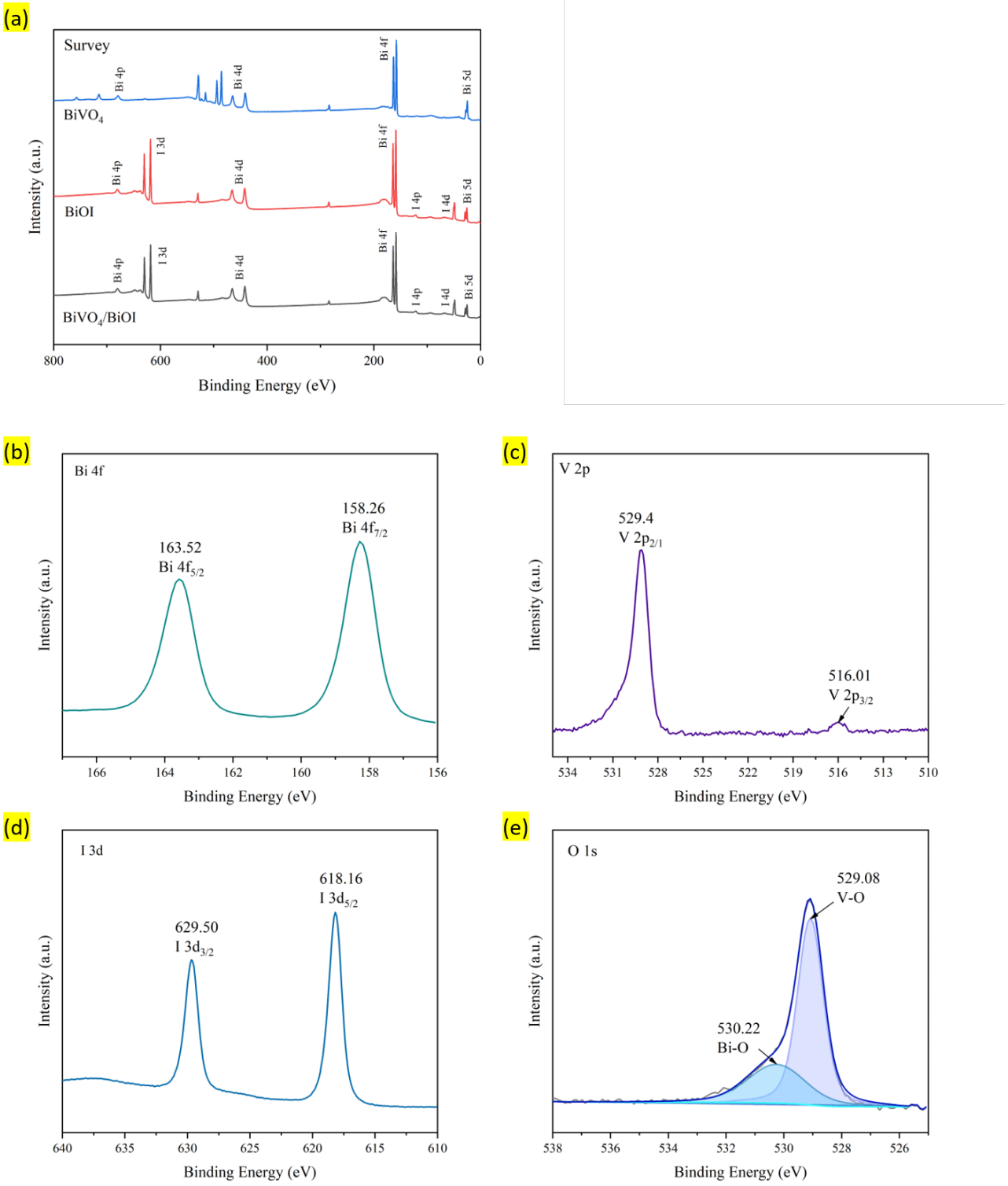

Figure 3.3: XPS spectra of the BiVO4, BiOI and $BiVO_4$/BiOI composite: (a) Survey, (b) Bi 4f, (c) V 2p, (d) I 3d and (e) O 1s.

3.2.2 XRD analysis

The results of the XRD analysis are summarised in Fig 3.4. Both diffraction peaks of $BiVO_4$ and BiOI can be significantly indexed as monoclinic scheelite BiVO4 and tetragonal BiOI phases match well with a JCPDS no. 75-1866 and JCPDS no. 01-073-2062 respectively. For monoclinic scheelite $BiVO_4$, the main peaks at 18.7^o, 19.0^o, 28.9^o, 30.5^o, 34.5^o, 35.2^o, 39.7^o, 42.4^o, 46.7^o, 47.2^o and 50.2^o corresponding to (101), (011), (112), (040), (200), (002), (211), (015), (204), (024), (116) planes respectively [15]. The characteristic peaks of tetragonal BiOI observed at $29.6442.4^o$, $31.6542.4^o$ and $45.3942.4^o$ have been indexed as the (102), (110) and (200) planes [16]. Further analysis showed that all the characteristic peaks were observed in $BiVO_4$/BiOI photoanode and no other impurity peaks were found in its phases, suggesting that BiOI was successfully electrodeposited on $BiVO_4$ layer, besides, pure phase and high crystallinity is achieved.

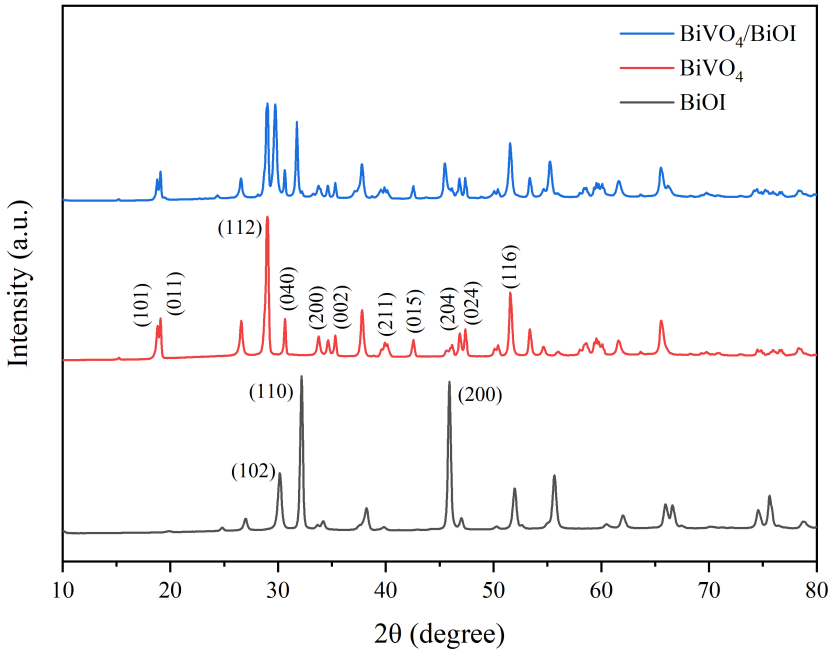

Figure 3.4: XRD patterns of the photoanodes: pure BiOI, pure $BiVO_4$, $BiVO_4$/BiOI.

3.2.3 SEM and EDS analysis

Fig 3.5 and 3.6 presented the further analysis of the morphology and composition of the photoanodes. Coral-like $BiVO_4$ structure was shown in Fig 3.5(a)(b)(c), it grew compactly from

the FTO glass. When electrodeposit the BiOI layer on $BiVO_4$ layer, the morphology of BiOI as small and thin discs covered the coral-like $BiVO_4$, which can be observed in Fig 3.5(d)(e)(f).

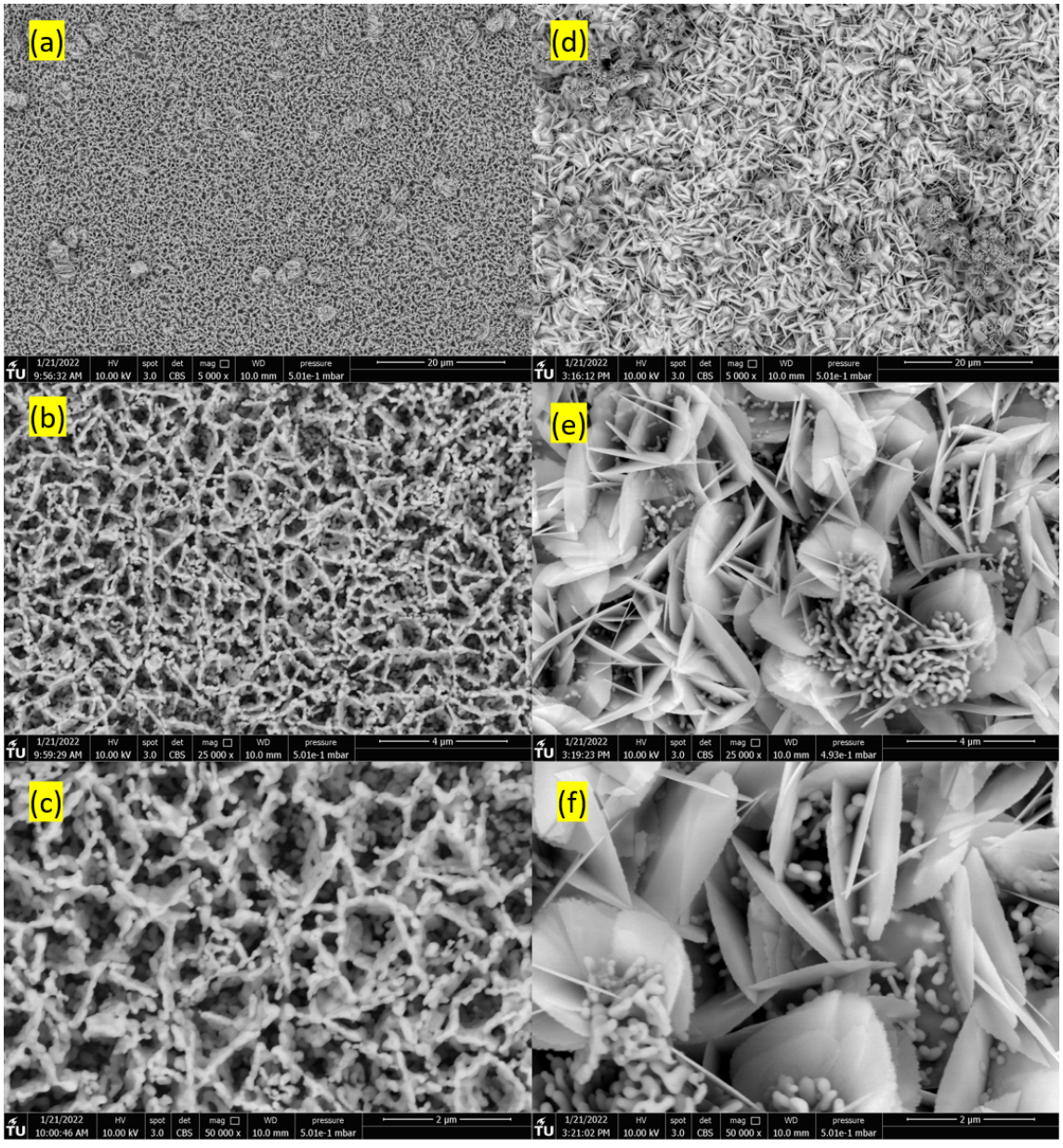

Figure 3.5: SEM images of the photoanodes: (a) 5000× $BiVO_4$, (b) 25000× $BiVO_4$, (c) 50000× $BiVO_4$, (d) 5000× $BiVO_4$/BiOI, (e) 25000× $BiVO_4$/BiOI, (f) 50000× $BiVO_4$/BiOI.

However, there was still $BiVO_4$ protruding from the disc BiOI, and their overall structure when combined resembles the petals and stamens of a flower, which indicates a successful synthesis of $BiVO_4$/BiOI heterojunction. The EDS spectra of $BiVO_4$/BiOI was shown in Fig 3.6, which also demonstrated the $BiVO_4$/BiOI heterojunction was successfully synthesized, because Bi, V, and I elements all homogeneously distributed in the composites. Further, the elements

characteristic signal peaks of Bi, I and V were observed , and no impurity peaks, which indicated the photoanode had a high purity and both BiOI and $BiVO_4$ existed in it.

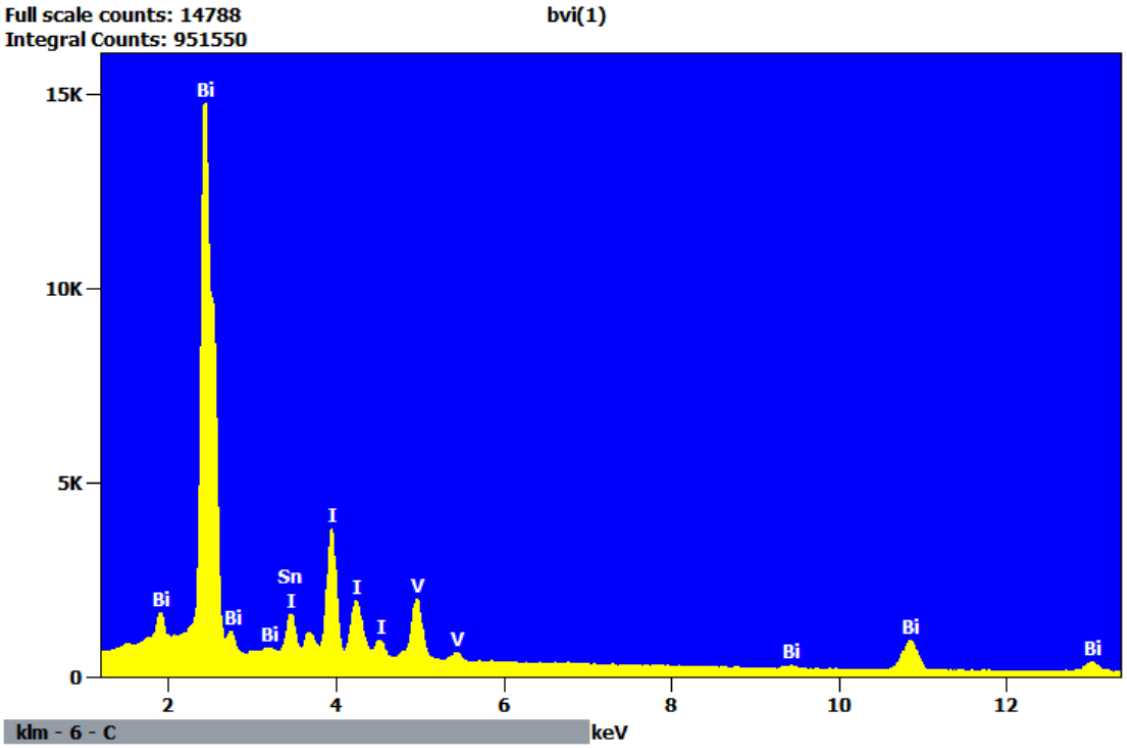

Figure 3.6: EDS spectrum of $BiVO_4$/BiOI.

3.3 Optical properties of the photoanodes

3.3.1 UV-vis analysis

UV-vis analysis was applied to measure the optical properties of the BiOI, $BiVO_4$ and $BiVO_4$/BiOI photoanodes, Fig3.7(a) represented the spectra of the absorb photons in the visible light region. When using the pure $BiVO_4$ and BiOI, the absorption edges can be traced to approx. 520 nm and 650 nm respectively. However, when synthesis of the heterojunction of $BiVO_4$/BiOI, the absorption edges increased to approx. 670 nm, which can be indicated that the heterojunction was able to take advantage of more solar energy, and produce more photogenerated electron-hole pairs under visible light.

In order to calculate the band gap energies of the crystalline semiconductors, the Tauc ap-

proach was used to estimate the pure BiOI and $BiVO_4$ as shown in Equation 3.1 [16, 17]:

$$\alpha h\upsilon = A(h\upsilon - E_g)^{n/2} \tag{3.1}$$

where,

$$\alpha = absorption\ coefficient,$$

$$h\upsilon = photon\ energy,$$

$$A = proportionality\ constant,$$

$$E_g = band\ gap,$$

$$n = 1\ for\ BiVO_4, 4\ for\ BiOI.$$

AS shown in Fig 3.7(b) the estimated band gap energies were 1.95 eV and 2.49 eV for BiOI and $BiVO_4$ respectively by the plot of $(\alpha h\upsilon)^2$ versus $h\upsilon$ and $(\alpha h\upsilon)^{1/2}$ versus $h\upsilon$, which were highly consistent with the previous reported data [18–20].

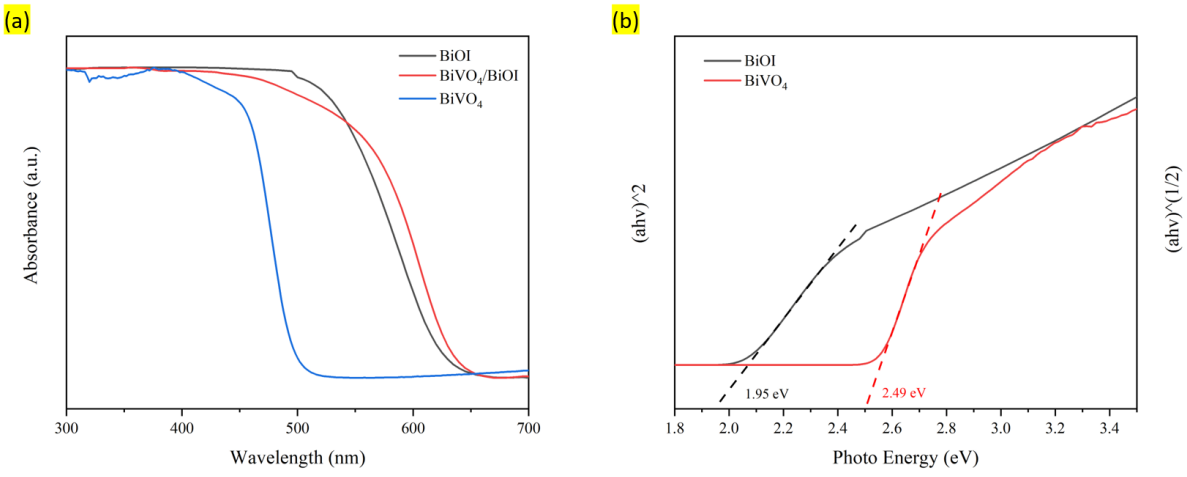

Figure 3.7: (a) The UV-vis absorbance spectra of BiOI, $BiVO_4$ and $BiVO_4$/BiOI, (b) The estimated band gap edges of pure BiOI and pure $BiVO_4$.

3.3.2 IPCE analysis

Further IPCE analysis revealed the contribution of photoanodes optical properties by the heterojunction of $BiVO_4$/BiOI. As shown in Fig 3.8, when applied 1 V potential bias on the photoanode

in the solution of 50 μg/L and 0.1 M Na_2SO_4, the IPCE result of 17% for $BiVO_4$/BiOI is significantly higher than the pure $BiVO_4$ in the wavelength ranging from 330 nm to 500 nm, which was strong evidence of the improvement of effective utilization of captured photons and inhibition of the combination of carriers on the photoanode surface [21].

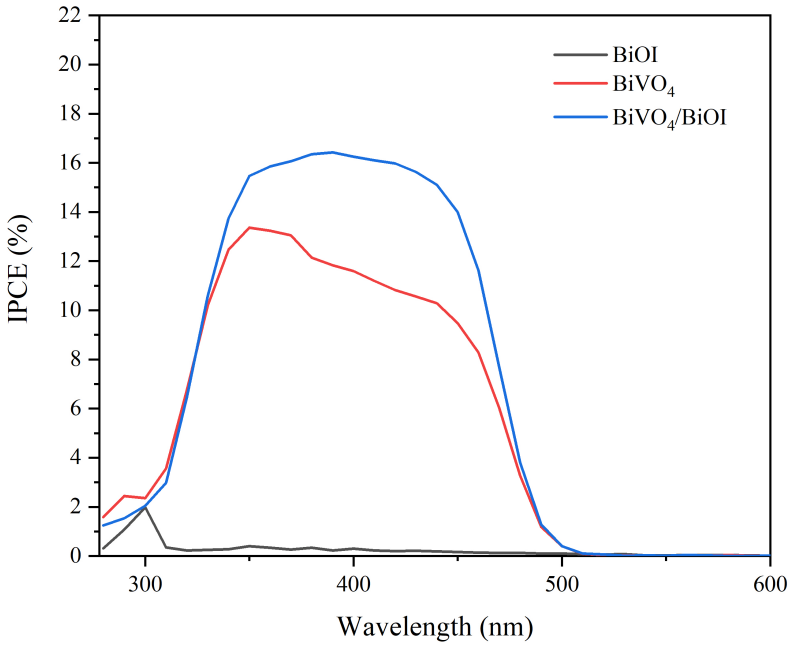

Figure 3.8: IPCE curve of BiOI, $BiVO_4$ and $BiVO_4$/BiOI photoanodes at the specified wavelength.

3.4 Photoelectrochemical and electrochemical analysis

3.4.1 LSV and photocurrent analysis

In order to further analyse the contribution of the $BiVO_4$/BiOI heterojunction, LSV measurements are carried out in a solution of 50 μg/L and 0.1 M Na_2SO_4 at a scan rate of 0.1 V/s and in both light and dark conditions. As shown in Fig 3.9 all of the current obtained in dark conditions was lower than what was observed in dark conditions. Surprisingly, comparing the photoanodes in the light condition, $BiVO_4$ photoanode had the highest photocurrent than $BiVO_4$/BiOI and other photoanodes before 1.3 V. However, this finding of the current study does not support the previous research. As mentioned in the literature review, $BiVO_4$/BiOI heterojunction should

increase the mobility of charge carriers under excitation by visible light [6].

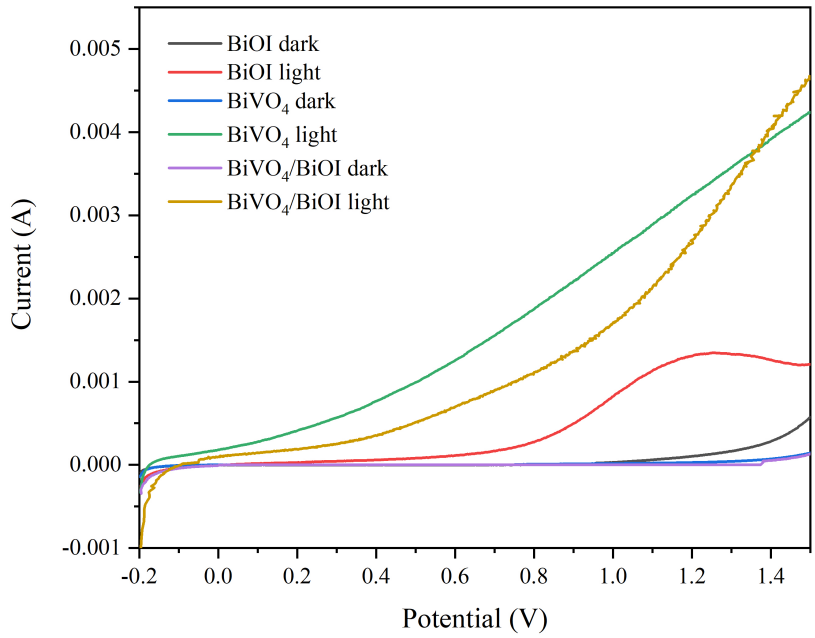

Figure 3.9: LSV plot of BiOI, $BiVO_4$ and $BiVO_4$/BiOI photoanodes at light and dark conditions.

In this case, to figure out the reason of the differs, the photocurrent was recored at an applied bias potential of 1 V, in a solution of 50 μg/L and 0.1 M Na_2SO_4. In the literature review, addition of OMP in the solution resulted in an increase of the recorded current, which means that OMP plays a functional role in the operation of the cell, for instance, through the consumption of the photogenerated holes that leads to its oxidation [22]. Consumption of the holes means that more free electrons are available and, consequently, a higher current. Contrary to expectations, this study still did not observed the higher photocurrent created by $BiVO_4$/BiOI heterojunction, the results are presented in Fig 3.10. Opposite to the previous research, 2.5 mA photocurrent of the $BiVO_4$ photoanode was twice as much as 1 mA of $BiVO_4$/BiOI heterojunction, which was also accords with our earlier observations of LSV analysis. This observation may support the hypothesis that the electrons generated by the photoanode under visible light irradiation, react with the disolved oxygen in the solution at a very fast rate to produce $^{\cdot}O_2^-$, which was highly oxidizing and immediately degradated the OMPs in the solution, hence there were not enough electrons to pass through the circuit and the photocurrent is reduced instead. These data must

be interpreted with caution because the bigger size of the photoanodes and the larger volume of the solution were used in this study, were all the sources of uncertainty. It can thus be suggested that the photocurrent of the photoanode is not a direct indicator for the OMPs degradation efficiency.

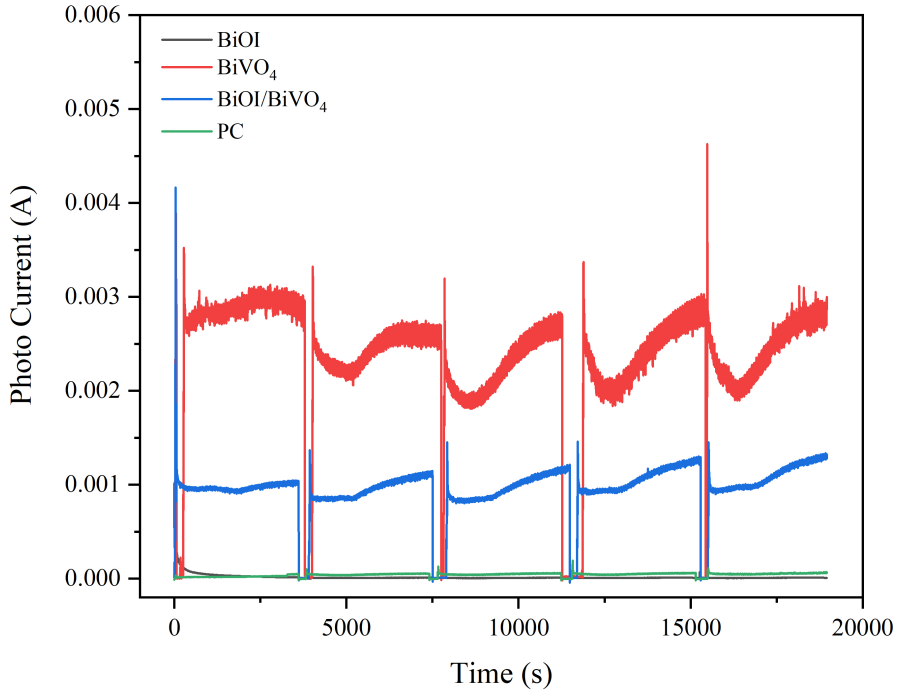

Figure 3.10: Photocurrent density versus time plots of BiOI, $BiVO_4$, $BiVO_4$/BiOI and photocatalysis of $BiVO_4$/BiOI during degradation experiments.

Nonetheless, the photocurrent of the $BiVO_4$ was not as stable as the one generated by $BiVO_4$/BiOI heterojunction. Also, both of the photocurrent curves fluctuated regularly with time in each sampling interval, it decreased to the bottom and then kept increasing until the end. Hence, it could conceivably be hypothesised that the higher photocurrent, the larger instability and volatility margin observed. Further, such connections likely exist between the magnetic field produced by the magnetic stirring system and the obtained photocurrent, the higher the current generated under the influence of the same magnetic field, the more significantly the current is affected and therefore the higher the current instability, which based on the Faraday's law of induction. The reason for the fluctuations could be hypothesised that the higher temperature can also increase the photocurrent. Because the ice was settled surrounding the degradation

cell to minimize the evaporation of solution, as the ice melted at first, it absorbs heat from the degradation cell, the solution temperature dropped and the photocurrent decreased, later the ice melted completely and the photocurrent increases following the overall temperature raised. Further research should be undertaken to investigate the factors influencing photocurrent.

3.4.2 EIS analysis

In the final part of the photoelectrochemical analysis, the EIS was carried out in both the acetaminophen solution of 50 μg/L and 3 mg/L with 0.1 M Na_2SO_4 at a bias potential of 1 V to further analyse the unexpected results.

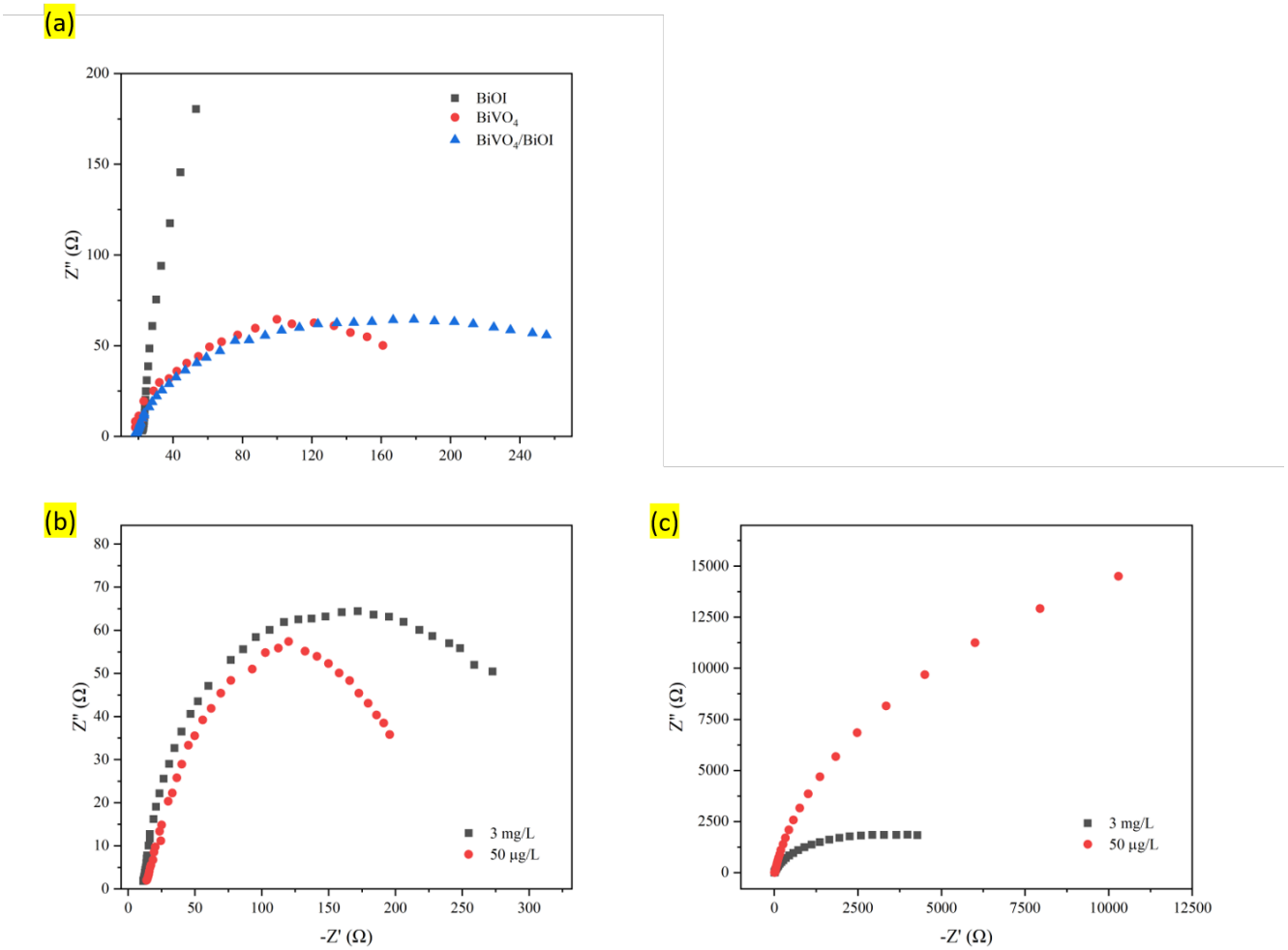

Figure 3.11: EIS plots of (a) BiOI, $BiVO_4$ and $BiVO_4$/BiOI photoanodes in 3 mg/L acetaminophen, only $BiVO_4$/BiOI photoanodes in (b) light condition and (c) dark condition when applied in 50 μg/L and 3 mg/L acetaminophen solution.

As shown in Fig 3.11(a), the charge-transfer resistance (R_{ct}) of each photoanodes can be obtained by the sense-circular arc. The difference between the BiOI, $BiVO_4$ and $BiVO_4$/BiOI photoanodes was significant, BiOI has the highest R_{ct} even if in the light condition owing to it had the largest semi-circular arc. Interestingly, the R_{ct} of $BiVO_4$ photoanode is higher than $BiVO_4$/BiOI, which has not previously been described. This observation may support the hypothesis that most of the electrons produced by $BiVO_4$/BiOI photoanode were rapidly joined the reaction of OMP degradation, therefore, fewer electrons existed and the obtained R_{ct} was higher.

Most studies in the field of EIS measurements have only focused on one concentration of the solution, this study applied the same photoanode in the acetaminophen solution of both 50 μg/L and 3 mg/L, in order to figure out the effect of OMPs concentration on R_{ct}, the light and dark results were presented in 3.11(a) and 3.11(b) respectively. For light conditions, both of the R_{ct} were relatively lower than the dark ones, however, the R_{ct} of 3 mg/L was higher than 50 μg/L. A possible explanation for this might be that the more OMPs existed in the solution, the more electrons were consumed by the OMPs degradation, and the higher R_{ct} would be obtained. Contrary to expectations, for the dark condition, even if there were no electrons created, both of the R_{ct} were close to infinity, and the R_{ct} of 3 mg/L was significantly lower than 50 μg/L. This inconsistency may be due to the photoanode in OMPs solution can be equated to a capacitor.

3.5 Photoelectrochemical degradation of Acetaminophen

To demonstrate the enhanced effect of $BiVO_4$/BiOI heterojunction on OMPs degradation, BiOI, $BiVO_4$ and $BiVO_4$/BiOI photoanodes were applied for the PEC degradation of 50 μg/L acetaminophen. The degradation process was performed at a bias potential of 1 V, with 0.1 M Na_2SO_4 as the electrolyte.

As shown in Fig 3.12 (a), after 120 min, the removal efficiencies of 15%, 67% and 87% were achieved by the BiOI, $BiVO_4$ and $BiVO_4$/BiOI photoanodes respectively for acetaminophen. This finding broadly supports the work of other studies in this area linking the enhancement of PEC degradation for OMPs with $BiVO_4$/BiOI heterojunction [6]. To further analyse the kinetics of the degradation, the pseudo-first-order kinetic equation ($y=e^{-kt}$) was fitted to the degradation data of each photoanodes was presented in Fig 3.12 (b). The reaction rate constant

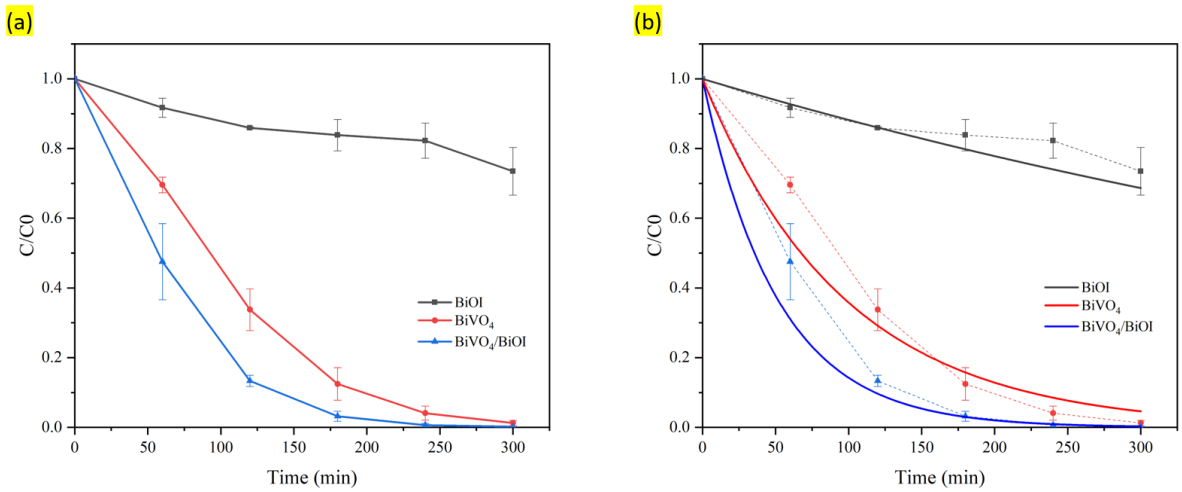

Figure 3.12: (a) Normalized concentration decay versus time plots, (b) Kinetics plots for degradation of BiOI, $BiVO_4$ and $BiVO_4$/BiOI photoanodes.

of 0.019 min^{-1} obtained from the $BiVO_4$/BiOI heterojunction was the highest one compared to 0.01 min^{-1} and 0.001 min^{-1} of BiOI and $BiVO_4$ photoanodes respectively. Based on these results, a positive correlation was found between $BiVO_4$/BiOI heterojunction and high OMPs degradation efficiency.

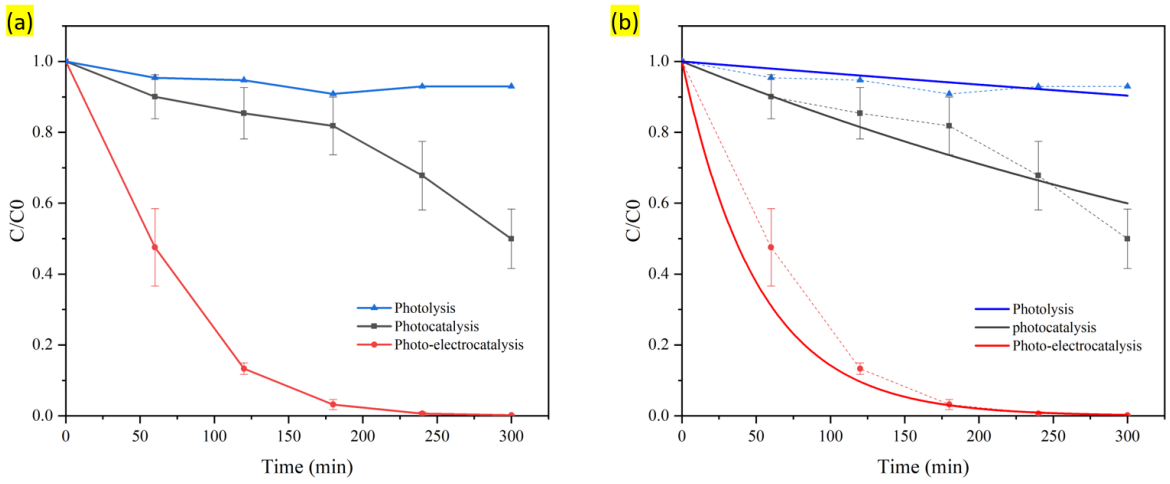

Figure 3.13: (a) Normalized concentration decay versus time plots, (b) Kinetics plots for degradation of photolysis, photocatalysis and photo-electrocatalysis.

However, previous studies mentioned photolysis and photocatalysis also had a high removal efficiency of OMPs [23, 24]. To further prove the results were obtained by PEC degradation only,

50 μg/L acetaminophen solution was degraded by photolysis and photocatalysis ($BiVO_4$/BiOI photoanode at a bias potential of 0 V). As shown in Fig 3.13 (a), in 3 hours degradation process, merely 7% and 50% achieved by photolysis and photocatalysis respectively, which means most of the acetaminophen was degraded by PEC activity. Furthermore, the kinetics data presented in Fig 3.13 (b) also proved this result. The reaction rate constants of 1.7×10^{-3} min^{-1} and 3.4×10^{-4} min^{-1} were fitted to the photolysis and photocatalysis reaction respectively and much slower than 0.019 min^{-1} of PEC reaction, which matched those observed in earlier studies. According to these data, we can infer that the generated holes are able to degrade the OMPs and also produce hydroxyl radicals by reacting with H_2O, then hydroxyl radicals can further degrade the OMPs. Besides, the applied bias potential can decrease the rate of charge carriers' recombination and improve the separation at the same time [25].

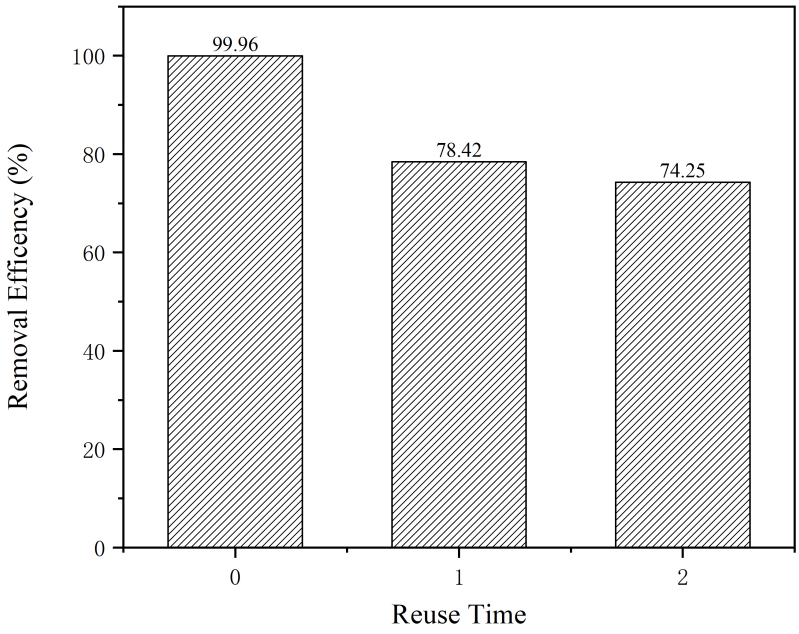

Figure 3.14: Circulating runs in the PEC degradation of 50 μg/L acetaminophen over $BiVO_4$/BiOI photoanodes.

This study reused the $BiVO_4$/BiOI photoanodes for another 2 cycles to check the reusability and stability of the photoanode. As can be seen from Fig 3.14, even if the photoanode ran 3 cycles and 18 hours in total, the removal efficiency presented no significant loss. It can therefore be assumed that the $BiVO_4$/BiOI photoanode is stable for an engineering application.

Chapter 4

Conclusions and Recommendations

This study has shown that $BiVO_4$/BiOI heterojunction can be conveniently prepared by electrodeposition technique on FTO glass. The second major finding was that $BiVO_4$/BiOI heterojunction can enhance the PEC activity, and further increase the degradation efficiency of the OMPs in demoralized water under visible light. It achieved 99% degradation efficiency in 3 hours and 0.019 min^{-1} of the reaction rate constant. Overall, the $BiVO_4$/BiOI heterojunction could be a possible application to remove the OMPs in WWTPs effluent under solar irradiation.

The question raised by this study is that the results of LSV, EIS and photocurrent were all observed fewer electrons existed. Considerably more work will need to be done to determine the reason why there were fewer electrons but still higher removal efficiency of OMPs, and which reactions would the electrons evolve in. Most studies of PEC degradation have only been carried out with the one photoanode which had the highest photocurrent result, but not degradation efficiency for each photoanode, therefore, such expositions are unsatisfactory. Further research in this field would be of great help in exploring the details of the reactions between the photoanodes and the OMPs.

Bibliography

[1] Guilherme Garcia Bessegato, Thaís Tasso Guaraldo, Juliana Ferreira de Brito, Michelle Fernanda Brugnera, and Maria Valnice Boldrin Zanoni. Achievements and trends in photoelectrocatalysis: from environmental to energy applications. *Electrocatalysis*, 6(5):415–441, 2015.

[2] Suqing Wu and Yun Hang Hu. A comprehensive review on catalysts for electrocatalytic and photoelectrocatalytic degradation of antibiotics. *Chemical Engineering Journal*, 409: 127739, 2021.

[3] Oscar Rozas, Cristiane Vidal, Carolina Baeza, Wilson F Jardim, Alfred Rossner, and Héctor D Mansilla. Organic micropollutants (omps) in natural waters: Oxidation by uv/h2o2 treatment and toxicity assessment. *Water research*, 98:109–118, 2016.

[4] Yunlong Luo, Wenshan Guo, Huu Hao Ngo, Long Duc Nghiem, Faisal Ibney Hai, Jian Zhang, Shuang Liang, and Xiaochang C Wang. A review on the occurrence of micropollutants in the aquatic environment and their fate and removal during wastewater treatment. *Science of the total environment*, 473:619–641, 2014.

[5] Robert Loos, Raquel Carvalho, Diana C António, Sara Comero, Giovanni Locoro, Simona Tavazzi, Bruno Paracchini, Michela Ghiani, Teresa Lettieri, Ludek Blaha, et al. Eu-wide monitoring survey on emerging polar organic contaminants in wastewater treatment plant effluents. *Water research*, 47(17):6475–6487, 2013.

[6] Benjamin O Orimolade, Babatunde A Koiki, Gbenga M Peleyeju, and Omotayo A Arotiba. Visible light driven photoelectrocatalysis on a fto/bivo4/bioi anode for water treatment involving emerging pharmaceutical pollutants. *Electrochimica Acta*, 307:285–292, 2019.

[7] Rimeh Daghrir, Patrick Drogui, and Didier Robert. Photoelectrocatalytic technologies for environmental applications. *Journal of Photochemistry and Photobiology A: Chemistry*, 238: 41–52, 2012.

[8] Benjamin O Orimolade and Omotayo A Arotiba. Bismuth vanadate in photoelectrocatalytic water treatment systems for the degradation of organics: a review on recent trends. *Journal of Electroanalytical Chemistry*, 878:114724, 2020.

[9] Xuelian Liu, Zhuang Guo, Linbi Zhou, Jin Yang, Hongbin Cao, Mei Xiong, Yongbing Xie, and Guangru Jia. Hierarchical biomimetic bivo4 for the treatment of pharmaceutical wastewater in visible-light photocatalytic ozonation. *Chemosphere*, 222:38–45, 2019.

[10] Basanth S Kalanoor, Hyungtak Seo, and Shankara S Kalanur. Recent developments in photoelectrochemical water-splitting using wo3/bivo4 heterojunction photoanode: A review. *Materials Science for Energy Technologies*, 1(1):49–62, 2018.

[11] Daimei Chen, Jinjin Yang, Yi Zhu, Yuanming Zhang, and Yongfa Zhu. Fabrication of bioi/graphene hydrogel/fto photoelectrode with 3d porous architecture for the enhanced photoelectrocatalytic performance. *Applied Catalysis B: Environmental*, 233:202–212, 2018.

[12] Olivier Monfort and Gustav Plesch. Bismuth vanadate-based semiconductor photocatalysts: a short critical review on the efficiency and the mechanism of photodegradation of organic pollutants. *Environmental Science and Pollution Research*, 25(20):19362–19379, 2018.

[13] Yongyang Chen, Yonggang Liu, Xin Xie, Chen Li, Yushan Si, Menghan Zhang, and Qishe Yan. Synthesis flower-like bivo4/bioi core/shell heterostructure photocatalyst for tetracycline degradation under visible-light irradiation. *Journal of Materials Science: Materials in Electronics*, 30(10):9311–9321, 2019.

[14] Shining Ni, Tiantian Zhou, Haonan Zhang, Yongqiang Cao, and Ping Yang. Bioi/bivo4 two-dimensional heteronanostructures for visible-light photocatalytic degradation of rhodamine b. *ACS Applied Nano Materials*, 1(9):5128–5141, 2018.

[15] Kunfeng Zhang, Yuxi Liu, Jiguang Deng, Shaohua Xie, Xingtian Zhao, Jun Yang, Zhuo Han, and Hongxing Dai. Co–pd/bivo4: High-performance photocatalysts for the degradation of

phenol under visible light irradiation. *Applied Catalysis B: Environmental*, 224:350–359, 2018.

[16] AA Abuelwafa, R Md Matiur, Anissa A Putri, and T Soga. Synthesis, structure, and optical properties of the nanocrystalline bismuth oxyiodide (bioi) for optoelectronic application. *Optical Materials*, 109:110413, 2020.

[17] Hyeonjin Kim, Kyunghyeon Yoo, Yongjun Kim, and Seog-Young Yoon. Thermochromic behaviors of boron–magnesium co-doped bivo4 powders prepared by a hydrothermal method. *Dyes and Pigments*, 149:373–376, 2018.

[18] Narges Omrani and Alireza Nezamzadeh-Ejhieh. Photodegradation of sulfasalazine over cu2o-bivo4-wo3 nano-composite: characterization and experimental design. *International journal of hydrogen energy*, 45(38):19144–19162, 2020.

[19] Teeradech Senasu, Sujittra Youngme, Khuanjit Hemavibool, and Suwat Nanan. Sunlight-driven photodegradation of oxytetracycline antibiotic by bivo4 photocatalyst. *Journal of Solid State Chemistry*, 297:122088, 2021.

[20] Ahmed Alzamly, Maram Bakiro, Salwa Hussein Ahmed, Sundus M Sallabi, Ruba Abdullah Al Ajeil, Shadha Ahmed Alawadhi, Huda Ahmed Selem, Shamma Saleh Mubarak Al Meshayei, Abbas Khaleel, Noura Al-Shamsi, et al. Construction of biof/bioi nanocomposites with tunable band gaps as efficient visible-light photocatalysts. *Journal of Photochemistry and Photobiology A: Chemistry*, 375:30–39, 2019.

[21] Can Li, Fan Feng, Jie Jian, Youxun Xu, Fan Li, Hongqiang Wang, and Lichao Jia. Boosting carrier dynamics of bivo4 photoanode via heterostructuring with ultrathin bioi nanosheets for enhanced solar water splitting. *Journal of Materials Science & Technology*, 79:21–28, 2021.

[22] Iosif Tantis, Leda Bousiakou, Zacharias Frontistis, Dionissios Mantzavinos, Ioannis Konstantinou, Maria Antonopoulou, George-Albert Karikas, and Panagiotis Lianos. Photocatalytic and photoelectrocatalytic degradation of the drug omeprazole on nanocrystalline titania films in alkaline media: effect of applied electrical bias on degradation and transformation products. *Journal of hazardous materials*, 294:57–63, 2015.

[23] Laleen C Bodhipaksha, Charles M Sharpless, Yu-Ping Chin, and Allison A MacKay. Role of effluent organic matter in the photochemical degradation of compounds of wastewater origin. *Water research*, 110:170–179, 2017.

[24] Dion Awfa, Mohamed Ateia, Manabu Fujii, Matthew S Johnson, and Chihiro Yoshimura. Photodegradation of pharmaceuticals and personal care products in water treatment using carbonaceous-tio2 composites: A critical review of recent literature. *Water research*, 142: 26–45, 2018.

[25] Sadhna Sadhna Jagannathan. Photoelectrocatalytic degradation of organic micropollutants in aqueous solutions using bismuth vanadate photoanodes. 2022.